


# Wetting transition in the transverse-field spin- $\frac{1}{2}$ XY model with boundary fields

Kun Hu<sup>\*</sup> and Xintian Wu<sup>†</sup>*Department of Physics, Beijing Normal University, Beijing 100875, China*
 (Received 3 November 2022; revised 20 March 2023; accepted 10 April 2023; published 25 April 2023)

The wetting transition in the transverse-field spin- $\frac{1}{2}$  XY model with opposite boundary fields  $h_L^x h_R^x < 0$  is studied analytically and numerically. We find that the phase diagram is complex and that the wetting transition is of three types: first, second, and fourth order. The energy gap is obtained analytically, and the magnetization profile, correlation functions, and wetting layer thickness are obtained numerically. For  $|h_L^x|, |h_R^x| < h_w$ , a first-order phase transition occurs at  $h_L^x = -h_R^x$ , where  $h_w$  is the continuous wetting transition point. For  $|h_R^x|$  larger than  $h_w$ , the continuous wetting transition occurs at  $h_L^x = h_w$ , and vice versa. For  $g \neq 1 - \gamma^2$ , the wetting transition is second order, and commensurate and incommensurate phases occur for  $g < 1 - \gamma^2$  and  $g > 1 - \gamma^2$ , respectively. For  $g = 1 - \gamma^2$ , the wetting transition is fourth order. For this fourth-order phase transition, the third derivative of the surface magnetization oscillates and diverges near the transition point. The correlation length exponent is  $\nu = 2$ , and the dynamic exponent is  $z = 2$ . Thus, this fourth-order transition belongs to a new universality class. The wetting behavior is induced by asymmetric boundary fields  $h_L^x = -h_R^x$  and its finite-size scaling is discussed.

DOI: [10.1103/PhysRevB.107.134433](https://doi.org/10.1103/PhysRevB.107.134433)

## I. INTRODUCTION

Zero-temperature quantum phase transitions are phenomena of considerable interest [1–3]. These transitions arise in many-body systems with competing ground states controlled by nonthermal parameters. They are continuous when the ground state of the system changes continuously at the transition point and correlation functions develop a divergent length scale. They are instead of first-order when ground-state properties are discontinuous across the transition point.

The one-dimensional XY model is a good testing ground for the quantum phase transition. In 1961 Lieb [4] solved exactly the XY model in the absence of a magnetic field, and Katsura [5] computed the spectrum of the XY model with magnetic field in 1962. The two-dimensional XY model was subsequently investigated using a variety of techniques [6]: the renormalization group [7,8], Monte Carlo simulations [9,10], perturbation theory [11], exact finite-lattice calculations [12,13], variational methods [14], and spin-wave theory [15,16]. The quantum dynamics [17] and entanglement [18–20] of the spin- $\frac{1}{2}$  XY chain in a transverse field have been extensively studied by scholars.

We studied the wetting transition in the transverse-field XY model with boundary fields and found many interesting phase transitions remain to be uncovered. The classical wetting transition has a long history and has attracted enormous theoretical and experimental interest [21,22]. The first quantitative scientific study on the wetting phenomenon was carried out in 1805 by T. Young, who introduced the concept of the contact angle and formulated the Young equation. Moldover

and Cahn performed experiments in 1980 demonstrating the existence of the wetting phase transition; that is, binary liquid mixtures below a consolute point  $T_c$  exhibit two-phase coexistence. When the temperature is lowered, one phase is adsorbed on the wall of the container and also completely infiltrates the gas-liquid interface. When the temperature is reduced to a finite temperature  $T_w$ , the phase forms droplets at the gas-liquid interface. In addition, due to the correspondence between Ising ferromagnets and lattice-gas models of gas-fluid systems [23], the wetting transition can be studied using Ising models with boundary fields. Over 40 years ago, Abraham obtained an exact solution to the wetting transition in the two-dimensional Ising model with boundary fields [24,25]. The quantum version of the Abraham model, the one-dimensional transverse Ising model with boundary fields, was recently studied [26–28].

In this paper, we study the quantum wetting transition in the transverse-field XY model with opposite boundary fields. Consider that the system is in the ordered phase. Due to the opposite boundary fields, there is an interface between the up-spins and down-spins.

Tuning one of the boundary fields causes the interface to unbind from the boundary at which the interface is localized. The unbinding of the interface is called the wetting transition. We solve the model analytically and numerically. The energy gap, boundary magnetization and susceptibility, and the correlation function and length are calculated. The corresponding critical exponents are obtained. The phase diagram is found to be similar to that for the one-dimensional transverse-field Ising model; i.e., the wetting transition can be both discontinuous and continuous. In addition, there is a continuous fourth-order wetting transition. For this fourth-order wetting transition, the third derivative of the boundary magnetization oscillates and diverges at the transition point. The oscillating

\*kunhu@mail.bnu.edu.cn

†wuxt@bnu.edu.cn

scaling function is obtained numerically for different lattice sizes. This result is rather interesting because oscillating divergence is rare. The correlation length exponent is  $\nu = 2$ , and the dynamic exponent is  $z = 2$ . This transition belongs to a new universality class.

Thirty years ago, Parry and Evans pointed out that the wetting behavior induced by asymmetric wall fields has a profound effect on all aspects of the phase equilibria of the confined fluid [29]. We also discuss the quantum wetting transition with asymmetric boundary fields and its finite-size scaling. In the model we study, this effect occurs around the end point of the first-order phase transition, i.e.,  $h_L^x = -h_R^x = h_w$ .

This paper is organized as follows. In Sec. II, we define the transverse-field spin- $\frac{1}{2}$  XY model with boundary fields and introduce our procedure to solve the model. In Sec. III, we discuss the phase diagram in detail qualitatively. In Secs. IV, V, and VI, the first-, second-, and fourth-order wetting transitions are presented, respectively. In Sec. VII, we study the finite-size effect on the end point of the first-order phase transition. Section VIII is a summary.

## II. THE SPIN- $\frac{1}{2}$ XY MODEL WITH BOUNDARY FIELDS AND THE SOLVING METHOD

The Hamiltonian of the one-dimensional transverse-field anisotropic spin- $\frac{1}{2}$  XY chain with boundary fields is given by

$$H = H_0 + H_b, \quad (1)$$

where

$$H_0 = -\sum_{i=1}^{N-1} \frac{1}{2} (J_i^x \sigma_i^x \sigma_{i+1}^x + J_i^y \sigma_i^y \sigma_{i+1}^y) - \frac{g}{2} \sum_{i=1}^N \sigma_i^z \quad (2)$$

is the usual transverse-field XY model and

$$\begin{aligned} J_i^x &= \frac{J_i}{2} (1 + \gamma_i), \\ J_i^y &= \frac{J_i}{2} (1 - \gamma_i), \end{aligned} \quad (3)$$

where  $\sigma_i^\alpha$  ( $\alpha = x, y, z$ ) are Pauli matrices,  $J_i$  are couplings, and  $\gamma_i$  are the anisotropy measures. The Hamiltonian  $H_0$  indicates there is an isotropic XY chain where  $J_i^x = J_i^y$  for  $\gamma_i = 0$  and an anisotropic XY chain for  $\gamma_i = \pm 1$ . The boundary field term  $H_b$  can be generally written as

$$H_b = -\frac{1}{2} (|h_L^x| \sigma_1^x - |h_R^x| \sigma_{N+1}^x), \quad (4)$$

where  $h_L^x, h_R^x$  are the left and right boundary longitudinal fields, respectively. As there is no particular significance for one boundary field being in the  $x$  direction and the other being in the  $y$  direction, this case will not be discussed. Here, the two boundary fields of the Hamiltonian only lie along the  $x$  direction for  $\gamma_0 = \gamma_N = 1$ .

Following well-known theories [26,30–32], we extend the chain by adding two additional spins at the 0 and  $N + 1$  sites. The corresponding effective Hamiltonian  $H_{e1}$  is given by

$$H_{e1} = H_0 - \frac{1}{2} (|h_L^x| \sigma_0^x \sigma_1^x + |h_R^x| \sigma_N^x \sigma_{N+1}^x). \quad (5)$$

As  $\sigma_0^x$  and  $\sigma_{N+1}^x$  are free from the transverse field, they commute with the effective Hamiltonian  $H_{e1}$  and can be

diagonalized simultaneously. The Hilbert space can be divided into four sectors labeled  $(1, 1)$ ,  $(1, -1)$ ,  $(-1, 1)$ , and  $(-1, -1)$ , where  $(s_0^x, s_{N+1}^x)$  are eigenvalues of  $\sigma_0^x$  and  $\sigma_{N+1}^x$ . The restriction of  $H_e$  to the four sectors gives rise to the Hamiltonian  $H$  with four cases of different signs of  $h_L^x, h_R^x$ . Here, we investigate the case  $h_L^x > 0, h_R^x < 0$  and the sector  $(1, -1)$ . The case  $h_L^x < 0, h_R^x > 0$  can be obtained by symmetry.

Then we perform the Jordan-Wigner transformation and define the fermionic operators

$$c_i^\dagger = (-1)^i \prod_{j=0}^{i-1} \sigma_j^z \sigma_i^+, \quad (6)$$

where  $\sigma^\pm = (\sigma^x \pm i\sigma^y)/2$  ( $i$  is the imaginary unit). The effective Hamiltonian becomes

$$H_e = \frac{gN}{2} + \sum_{i,j=0}^{N+1} \left[ c_i^\dagger A_{ij} c_j + \frac{1}{2} c_i^\dagger B_{ij} c_j^\dagger - \frac{1}{2} c_i B_{ij} c_j \right], \quad (7)$$

where  $A$  and  $B$  are symmetric and antisymmetric matrices, respectively. Generally, the physical quantities  $J_i$  and  $\gamma_i$  can be arbitrary. However, in this study, we only consider uniform quantities: the couplings  $J_i = J = 1$  and the anisotropy  $\gamma_i = \gamma$ , where  $i = 1, 2, \dots, N - 1$ . Only  $h_L^x, h_R^x$  need to be assigned individually.

For clarity, we explicitly write the matrix elements for  $N = 4$  as follows:

$$A = \frac{1}{2} \begin{pmatrix} 0 & -|h_L^x| & 0 & 0 & 0 & 0 \\ -|h_L^x| & -2g & -J & 0 & 0 & 0 \\ 0 & -J & -2g & -J & 0 & 0 \\ 0 & 0 & -J & -2g & -J & 0 \\ 0 & 0 & 0 & -J & -2g & -|h_R^x| \\ 0 & 0 & 0 & 0 & -|h_R^x| & 0 \end{pmatrix},$$

$$B = \frac{1}{2} \begin{pmatrix} 0 & -|h_L^x| & 0 & 0 & 0 & 0 \\ |h_L^x| & 0 & -J\gamma & 0 & 0 & 0 \\ 0 & J\gamma & 0 & -J\gamma & 0 & 0 \\ 0 & 0 & J\gamma & 0 & -J\gamma & 0 \\ 0 & 0 & 0 & J\gamma & 0 & -|h_R^x| \\ 0 & 0 & 0 & 0 & |h_R^x| & 0 \end{pmatrix}.$$

We perform a Bogoliubov transformation by introducing new canonical fermionic variables:

$$\eta_k = \sum_{i=0}^{N+1} (g_{k,i} c_i + h_{k,i} c_i^\dagger). \quad (8)$$

These variables can be used to diagonalize the Hamiltonian. The coefficients  $g_{k,i}$  and  $h_{k,i}$  satisfy the following equations:

$$g_{k,i} = \frac{\psi_{k,i} + \phi_{k,i}}{2}, \quad h_{k,i} = \frac{\phi_{k,i} - \psi_{k,i}}{2}, \quad (9)$$

where  $\psi_{k,i}$  is the eigenvector of the matrix  $D$ :

$$D \equiv (A + B)(A - B), \quad D\psi_k = \varepsilon_k^2 \psi_k, \quad (10)$$

and

$$\phi_k = (A - B)\psi_k / \varepsilon_k. \quad (11)$$

In the equation presented above,  $\varepsilon_k \neq 0$ . Then, we explicitly write the elements of the matrix  $D$  for  $N = 4$ :

$$D = \frac{1}{4} \begin{pmatrix} 4|h_L^x|^2 & 4g|h_L^x| & 2|h_L^x|(1-\gamma) & 0 & 0 & 0 \\ 4g|h_L^x| & 4g^2 + (1+\gamma)^2 & 4g & 1-\gamma^2 & 0 & 0 \\ 2|h_L^x|(1-\gamma) & 4g & 4g^2 + 2(1+\gamma^2) & 4g & 1-\gamma^2 & 0 \\ 0 & 1-\gamma^2 & 4g & 4g^2 + 2(1+\gamma^2) & 4g & 0 \\ 0 & 0 & 1-\gamma^2 & 4g & 4g^2 + (1-\gamma)^2 + 4|h_R^x|^2 & 0 \\ 0 & 0 & 0 & 0 & 0 & 0 \end{pmatrix}. \quad (12)$$

To study the wetting phase transition [27,28], we set the boundary fields  $h_L^x > 0$ ,  $h_R^x < 0$  in the opposite direction. For the Hamiltonian  $H$  with  $h_L^x > 0$ ,  $h_R^x < 0$ , the ground state and the first excited state of  $H$  are the first and second excited states of the effective Hamiltonian  $H_{e1}$ , respectively. These states belong to the sector  $(1, -1)$  and are given by

$$|\Psi_1\rangle = \eta_1^\dagger |\Psi_0\rangle, \quad |\Psi_2\rangle = \eta_2^\dagger |\Psi_0\rangle. \quad (13)$$

The energy gap is given by the difference between the energies of these two states:  $\Delta = \varepsilon_2 - \varepsilon_1$ .

There is clearly a zero eigenvalue  $\varepsilon_0 = 0$  for the matrix  $D$  in Eq. (12). The zero mode is not related to the spectrum of the Hamilton  $H$ , and only the nonzero modes are relevant. There are  $N + 1$  nonzero modes that we label by  $k = 1, 2, \dots, N + 1$ . Here,  $0 = \varepsilon_0 < \varepsilon_1 < \varepsilon_2 \dots \varepsilon_{N+1}$ .

To calculate the correlation function  $C_{i,j}^x$ , we define two new operators [4]:

$$A_i = c_i^\dagger + c_i, \quad B_i = c_i^\dagger - c_i. \quad (14)$$

We obtain the correlation function [4] for the ground state  $|\Psi_1\rangle$  of the Hamiltonian  $H$  with  $h_L^x > 0$ ,  $h_R^x < 0$ :

$$\begin{aligned} \langle \Psi_1 | \sigma_i^x \sigma_j^x | \Psi_1 \rangle &= \langle \Psi_1 | B_i A_{i+1} B_{i+1} \dots A_{j-1} B_{j-1} A_j | \Psi_1 \rangle \\ &= \begin{vmatrix} G_{i,i+1} & G_{i,i+2} & \dots & G_{i,j} \\ G_{i+1,i+1} & G_{i+1,i+2} & \dots & G_{i+1,j} \\ \dots & \dots & \dots & \dots \\ G_{j-1,i+1} & G_{j-1,i+2} & \dots & G_{j-1,j} \end{vmatrix}, \end{aligned} \quad (15)$$

where  $j > i$ , and we define the contractions of pairs from Eqs. (13) and (14):

$$\begin{aligned} G_{i,j} &= \langle \Psi_1 | B_i A_j | \Psi_1 \rangle = -\langle \Psi_1 | A_j B_i | \Psi_1 \rangle \\ &= \psi_{1,i} \phi_{1,j} - \sum_{k=2}^{N+1} \psi_{k,i} \phi_{k,j}. \end{aligned} \quad (16)$$

As  $\sigma_0^x$  commutes with  $H_{e1}$ , the magnetization of the  $i$ th spin is related to the correlation function given by

$$m_i^x = \langle \Psi_1 | \sigma_i^x | \Psi_1 \rangle = \frac{1}{s_0^x} \langle \Psi_1 | \sigma_0^x \sigma_i^x | \Psi_1 \rangle. \quad (17)$$

Due to  $\sigma_0^x \sigma_1^x = B_0 A_1$ , the boundary magnetization of  $\sigma_1^x$  is given by [28]

$$m_1^x = \frac{1}{s_0^x} \left[ \psi_{1,0} \phi_{1,1} - \sum_{k=2}^{N+1} \psi_{k,0} \phi_{k,1} \right]. \quad (18)$$

Therefore, we can calculate the magnetization and the correlation function for all cases of  $h_L^x, h_R^x$  with different signs.

### III. PHASE DIAGRAM

The state we study is ordered; i.e., the spontaneous symmetry breaking occurs. Specifically it is given that  $0 < g < 1$ .

The phase diagram is quite complex since there four parameters:  $h_L^x, h_R^x, g$ , and  $\gamma$ . In order to give readers a clear picture, we discuss it qualitatively here.

For given  $g$  and  $\gamma$ , the phase diagram is sketched in Fig. 1. The point  $O$  ( $h_L^x = 0, h_R^x = 0$ ) is the original point. The parameter plane is divided into four parts. The boundaries of the four parts are represented by the red and blue solid lines. The situation in the second quadrant is symmetric to that in the fourth quadrant (see Fig. 1(b) in Ref. [27]).

The red solid line is given by  $h_L^x = -h_R^x$  for  $|h_L^x|, |h_R^x| < h_w$ , where  $h_w$  depends on the parameter  $g$  and  $\gamma$  and is the continuous wetting transition point. The blue solid lines in the fourth quadrant are given by  $h_L^x = h_w$  for  $h_R^x < -h_w$  and  $h_R^x = -h_w$  for  $h_L^x > h_w$ .

The situation in the first quadrant can be understood easily. Since  $h_L^x, h_R^x > 0$ , the ground state should have  $m_i^x > 0$  for all spins. Therefore we call that phase ‘‘positive.’’ Similarly the ground state in the third quadrant, where  $h_L^x, h_R^x < 0$ , has  $m_i^x < 0$  for all spins. So we call it the ‘‘negative’’ phase.

The situations in the second and fourth quadrant are subtle. Since the boundary fields are opposite, the magnetization

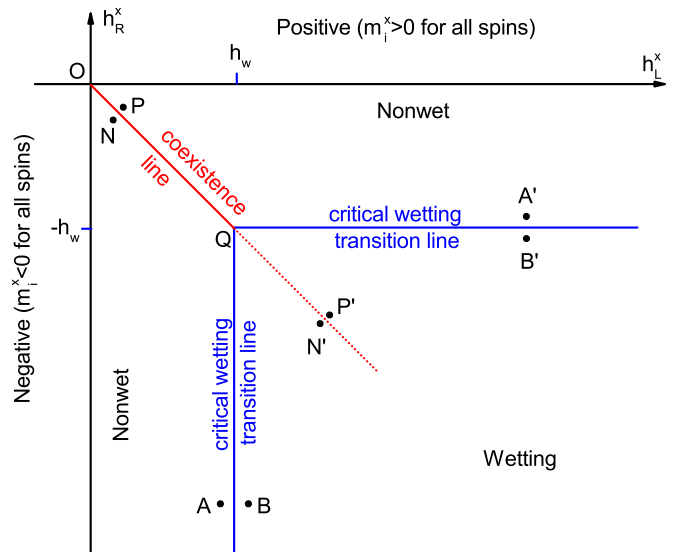


FIG. 1. The phase diagram for given  $g$  and  $\gamma$ .

should be positive (negative) at the left side of the spin chain and negative (positive) at the right. There should be an interface between the spins with positive and negative magnetization in the spin chain. Without calculation we can be sure that the interface is just at the middle of the spin chain for  $h_L^x = -h_R^x$  based on the symmetry.

At the nonwet region, whose boundaries are the negative  $h_R^x$  axis, the coexistence line (the red solid line), and the vertical critical wetting transition line (the vertical blue solid line), the interface is pinned at the left end of the spin chain. The number of spins with positive magnetization is finite. The number of the spins with positive magnetization can be called the positive layer thickness. At the vertical wetting transition line, the positive layer thickness diverges. This phase transition is continuous. It is the quantum version of the wetting transition on the two-dimensional Ising model or Abraham's model [25]. At the nonwet region, whose boundaries are the positive  $h_L^x$  axis, the coexistence line, and the horizontal critical wetting transition line, the interface is pinned at the right end of the spin chain. The number of spins with negative magnetization is finite. We call the number of the spins with negative magnetization the negative layer thickness. At the vertical wetting transition line, the negative layer thickness diverges. We study this kind of phase transition in Secs. V, VI, and VII.

As the boundary fields vary from the point  $N$  to  $P$  close to the coexistence line, the interface change discontinuously. The phase transition is the first order. Considering that the points  $N$  and  $P$  are very close, say their coordinates  $(h_L^x, h_R^x)$  are given by  $(h_1 + \delta, -h_1)$  and  $(h_1, -h_1 - \delta)$ , respectively, where  $0 < \delta \ll 1$  and  $0 < h_1 < h_w$ . The two points are very close, but the two phases are very different. Their magnetization profiles are totally different [see Figs. 3(b), 18(a)]. At point  $N$ , the interface is pinned at the left end of the spin chain, since the absolute value of  $h_L^x$  is larger than that of  $h_R^x$  and the left boundary field dominates. On the contrary, at the point  $P$ , the interface is pinned at the right end of the spin chain since the absolute value of  $h_R^x$  is larger than that of  $h_L^x$  and the right boundary field dominates. In the terminology of classical wetting transition, the two states of  $N$  and  $P$  can be called dry and wet phases.

As the boundary fields vary from the point  $N$  to  $P$ , the interface jumps from the left end to the right end of the boundary. In the thermodynamic limit, the change in the interface position is infinitely large, so the phase transition is the first order. We study this phase transition in Sec. IV.

Why is the red line called the coexistence line? Take the points  $N$  to  $P$  as a example. Suppose that we set  $h_L^x = -h_R^x$  on a real spin chain experimentally. Practically there is always an environmental noise. Assuming the noise intensity on the boundary fields is  $\delta$ , then the boundary fields can be  $N$  or  $P$ , which correspond two very different phases. Therefore under the surface fields  $h_L^x = -h_R^x$ , both phases can exist.

As a comparison, we see the points  $N'$  to  $P'$  close to the red dashed line, which is the extended one of the red line. Because the two points are in the wetting region, the interface is far away from both boundaries. In fact, close to the red dashed line, the interface is just at the middle of the spin chain. Minor deviation from the red dashed line can induce minor shift of the interface, so points  $N'$  to  $P'$  correspond to the same phase. In this case only one phase exists.

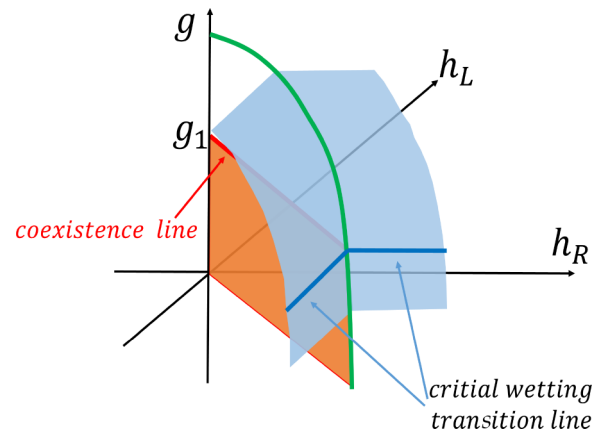


FIG. 2. The 3-dimensional sketch map of phase diagram for a given  $\gamma$ .

The point  $Q$  is the end point of the first-order phase transition, and also the transition point from the coexistence of two phases, in which the interface is pinned at the right end or the left end of the spin chain, to one phase, in which the interface is located at the middle of the spin chain. Parry and Evans pointed out that the wetting behavior induced by asymmetric wall fields has a profound effect on all aspects of the phase equilibria of the confined fluid 30 years ago [29]. Similar effects in the quantum wetting model should occur near by the point  $Q$ . We study them in Sec. VII.

The 3-dimensional phase diagram for a given  $\gamma$  is sketched in Fig. 2. The green solid curve is given by  $h_L^x = -h_R^x = h_w(g, \gamma)$ . The two leaves of gray curved surfaces are composed of wetting transition lines shown with solid blue lines in Fig. 1. The orange surface is composed of the coexistence line shown with the solid red line in Fig. 1. The red solid line and the blue solid lines are in the same plane given by  $g = g_1$ . Figure 1 is just such a plane.

The ordered state in the XY model without boundary fields has been obtained by Lieb *et al.* [4,5]. There are two types: the commensurate phase for  $g > 1 - \gamma^2$  and incommensurate phase [33] for  $g < 1 - \gamma^2$ . It is found that the wetting transition for the two phases belongs to the same universality although there are differences in terms of detail. However for  $g = 1 - \gamma^2$ , we find that the wetting transition is fourth order. This is a very interesting result.

#### IV. FIRST-ORDER PHASE TRANSITION ACROSS THE COEXISTENCE LINE

In this section, we study the first-order phase transition across the red solid line in Fig. 1.

There are two types of eigenvectors for the matrix  $D$  in Eq. (10): extended and localized states. For  $h_L^x, |h_R^x| < h_w$ , two localized states exist at the two boundaries; the competition between these localized states induces the first-order phase transition. In the limit of  $N \rightarrow \infty$ , these eigenvectors for the state localized at the left end are given by

$$\begin{aligned} \psi_{L,0} &= \frac{1 + \gamma}{2|h_L^x|} (c_1 x_1^2 + c_2 x_2^2), \\ \psi_{L,i} &= (-1)^i (c_1 x_1^{2-i} + c_2 x_2^{2-i}), \quad 1 \leq i. \end{aligned} \quad (19)$$



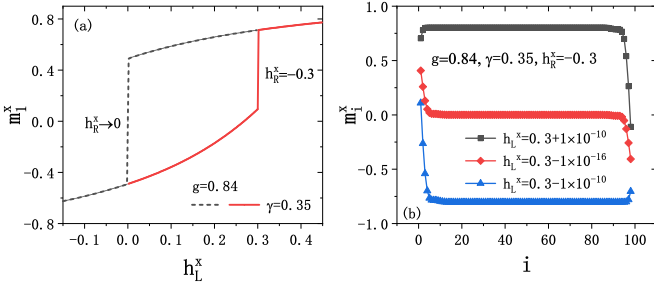


FIG. 3. (a) First-order phase transition across the border with  $g = 0.84$ . (b) Magnetization profiles around the first-order phase transition at  $h_L^x = |h_R^x|$  with  $h_R^x = -0.3$ ,  $g = 0.84$ , and  $N = 100$ .

The eigenvectors for the state localized at the right end are given by

$$\begin{aligned} \psi_{R,N+1} &= -\frac{1+\gamma}{2|h_R^x|} (d_1 x_1^2 + d_2 x_2^2), \\ \psi_{R,N-i} &= (-1)^{N-i} (d_1 x_1^{1-i} + d_2 x_2^{1-i}), \quad 0 \leq i, \end{aligned} \quad (20)$$

where  $c_1, c_2, d_1$ , and  $d_2$  are normalization constants, and the eigenvalues of the localized states are given by

$$\varepsilon = \sqrt{\frac{1}{4} \left[ (1-\gamma^2) \left(x + \frac{1}{x}\right)^2 - 4g \left(x + \frac{1}{x}\right) + 4(g^2 + \gamma^2) \right]}. \quad (21)$$

$x_1$  and  $x_2$  satisfy  $\varepsilon^2(x_1) = \varepsilon^2(x_2)$  in Eq. (21), where  $x_1, x_2$  can be complex numbers and  $|x_1|, |x_2| > 1$  guarantee the state to be localized.

The eigenvalues of the localized eigenstates at both ends are given by (see the Appendix)

$$\varepsilon_{L,R} = \sqrt{g^2 + \gamma^2 - \frac{2g\beta_{L,R}}{\sqrt{\alpha_{L,R}(1-\gamma^2)}} + \frac{\beta_{L,R}^2}{\alpha_{L,R}}}, \quad (22)$$

where

$$\alpha_{L,R} = (1+\gamma)^2 - 4h_{L,R}^x{}^2, \quad \beta_{L,R} = 1 + \gamma - 2h_{L,R}^x{}^2. \quad (23)$$

Equation (22) shows that the difference in the eigenvalues of the localized states at both ends only depends on the difference between the boundary fields  $h_L^x, h_R^x$ , and  $\varepsilon_L^2 = \varepsilon_R^2$  for  $|h_L^x| = |h_R^x|$ . These two eigenvectors are just the first and second excited states defined in Eq. (13). The corresponding eigenvalues are given by  $\varepsilon_1 = \min(\varepsilon_L, \varepsilon_R)$  and  $\varepsilon_2 = \max(\varepsilon_L, \varepsilon_R)$ . As we change  $h_L^x$  from  $h_L^x < -h_R^x$  to  $h_L^x > -h_R^x$ , the two levels cross, then the first-order phase transition occurs. The energy gap closes at the transition point  $h_L^x = -h_R^x$  in the thermodynamic limit.

In addition, some physical quantities such as the boundary magnetization  $m_1^x$  show discontinuity. The discontinuity can be shown rigorously in the exact solution. However it can be shown approximately in a large-size system, which can be solved numerically. For a system with size  $N = 100$ , we solve the matrix  $D$  numerically, and calculate the magnetization. We show the results in Fig. 3.

The discontinuity in boundary magnetization  $m_1^x$  is shown in Fig. 3(a). It exhibits a jump at  $h_L^x = |h_R^x|$  as we fix

TABLE I. Fitting coefficients for different lattice sizes.

Lattice size	$\delta$	$\Delta_0$	$\Delta_{m1}$
$N = 20$	$7.536 \times 10^{-4}$	$9.230 \times 10^{-4}$	0.308
$N = 30$	$2.817 \times 10^{-5}$	$3.447 \times 10^{-5}$	0.308
$N = 40$	$1.035 \times 10^{-6}$	$1.281 \times 10^{-6}$	0.308
$N = 60$	$1.396 \times 10^{-9}$	$1.735 \times 10^{-9}$	0.308
$N = 70$	$5.079 \times 10^{-11}$	$6.308 \times 10^{-11}$	0.308

$h_R^x = 0, -0.3$  and change  $h_L^x$ . The discontinuous phase transition is exhibited clearly.

We also calculate the magnetization profile  $m_i^x$ ,  $1 \leq i \leq N$  with  $N = 100$ , which is shown in Fig. 3(b). The magnetization profiles show a dramatic change as we change  $h_L^x$  in the very immediate vicinity of  $h_L^x = 0.3$ .

As shown in Fig. 3(b), the magnetization profiles for  $h_L^x = 0.3 + 1.0 \times 10^{-10}$  and  $h_L^x = 0.3 - 1.0 \times 10^{-10}$  are totally different. For  $h_L^x = 0.3 + 1.0 \times 10^{-10}$ , of which absolute value is bigger than that of the right boundary field  $h_R^x = -0.3$ , the magnetization is positive for the majority of the spins and the interface is pinned at the right end of the spin chain. We call this state the ‘‘positive’’ phase. On the contrary, for  $h_L^x = 0.3 - 1.0 \times 10^{-10}$ , of which the absolute value is less than that of the right boundary field  $h_R^x = -0.3$ , the magnetization is negative for the majority of the spins and the interface is pinned at the left end of the spin chain. We call this state the ‘‘negative’’ phase. In addition, we show the magnetization profile for  $h_L^x = 0.3 - 1.0 \times 10^{-16}$ , where two boundary fields can be regarded as asymmetric rigorously since  $10^{16}$  is the machine precision. Only in this case the interface is located at the center of the spin chain.

As one can see, the system transits from the positive phase to negative phase in the interval of  $h_L^x$  less than  $2.0 \times 10^{-10}$ . In fact, since there is always an environmental noise, we cannot set the absolute values of the two boundary fields to be equal exactly. Hence the system can be in the positive phase or negative phase. Therefore, we call the red line in Fig. 2 the coexistence line. It is well known that in the first-order phase transition between liquid and solid or liquid and gas, there is always a coexistence of two phases. Here in the quantum phase transition between positive and negative, there is a coexistence of two phases.

Based on the numerical results the finite-size scaling of the first-order phase transition is investigated. We calculate the eigenvalue of matrix  $D$  and the surface magnetization  $m_1^x$  for size  $N = 20, 30, 40, 60, 70$  with  $g = 0.84, \gamma = 0.4$ , and  $h_R^x = -0.3$ . We change the left boundary field  $h_L^x$  from 0.29 to 0.31. The energy gap and surface magnetization  $m_1^x$  are shown in Fig. 4.

Figures 4(a) and 4(b) show the numerical results for the energy gap  $\Delta = \varepsilon_2 - \varepsilon_1$  and the boundary magnetization  $m_1^x$  for  $g = 0.84$  and  $h_R^x = -0.3$ , respectively; panels (c) and (d) show their rescaled images.

The value of  $\Delta_0 = \Delta(h_L^x)|_{h_L^x = -h_R^x}$  is given in Table I and decreases as the lattice size increases. Through numerical calculation and data fitting, we verify that the energy gap  $\Delta$

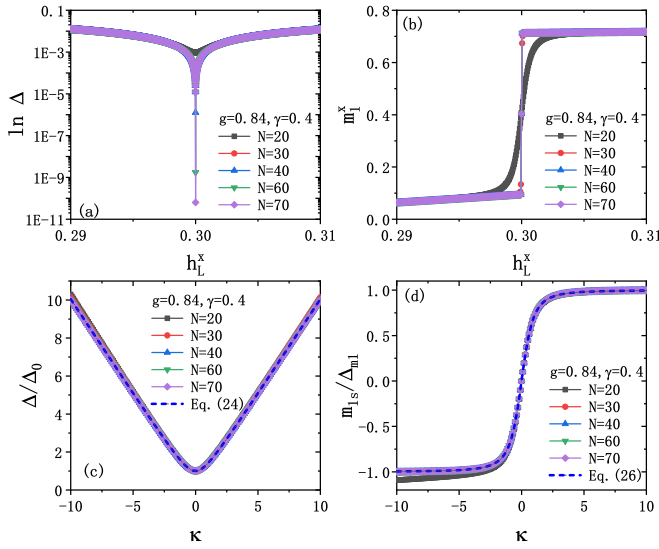


FIG. 4. (a) Numerical results for the energy gap  $\Delta$  for different lattice sizes with  $h_R^x = -0.3$ . (b) Numerical results for the boundary magnetization  $m_1^x$  for different lattice sizes with  $h_R^x = -0.3$ . (c) Rescaled energy gaps approach the scaling relation. (d) The rescaled singular parts of the boundary magnetization  $m_{1s}$  approach the scaling relation.

satisfies the scaling relation

$$\Delta = \Delta_0 \sqrt{1 + \kappa^2}, \quad (24)$$

where  $\kappa = \frac{h_L^x - |h_R^x|}{\delta}$  is the scaling variable. This scaling ansatz is proposed by Compostrini *et al.* [34] and verified in the transverse-field Ising model with surface fields [27]. The data collapse on the above scaling relation is shown in Fig. 4(c). Then,  $\delta$  can be obtained by data fitting. This is shown in Table I. In fact, we can call  $\delta$  the width of the phase transition, beyond which the two phases can be distinguished clearly. We simply fit the relation between  $\delta$  and  $N$ , and we get  $\delta \sim e^{-0.342N}$ . This means the width of the phase transition decreases exponentially with the system size  $N$ .

To further study the boundary magnetization jump, we define the singular boundary magnetization as

$$m_{1s} = m_1^x - m_{10}^x, \quad (25)$$

where  $m_{10}^x$  is the boundary magnetization at the transition point  $h_L^x = h_R^x$ . In addition  $m_{1s}^x$  satisfies the scaling relation [27]

$$m_{1s} = \Delta_{m1} \frac{\kappa}{\sqrt{1 + \kappa^2}}, \quad (26)$$

where  $\Delta_{m1}$  is the amplitude of the boundary magnetization jump. For different sizes, the fitted values of  $\Delta_{m1}$  are given in Table I. Figure 4(d) shows the data collapse to the aforementioned scaling relation.

## V. SECOND-ORDER PHASE TRANSITION: THE WETTING TRANSITION FOR $g \neq 1 - \gamma^2$

In this section, we study the continuous wetting transition across the blue solid lines in Fig. 1. As discussed in last section, there exist localized states. However the existence of

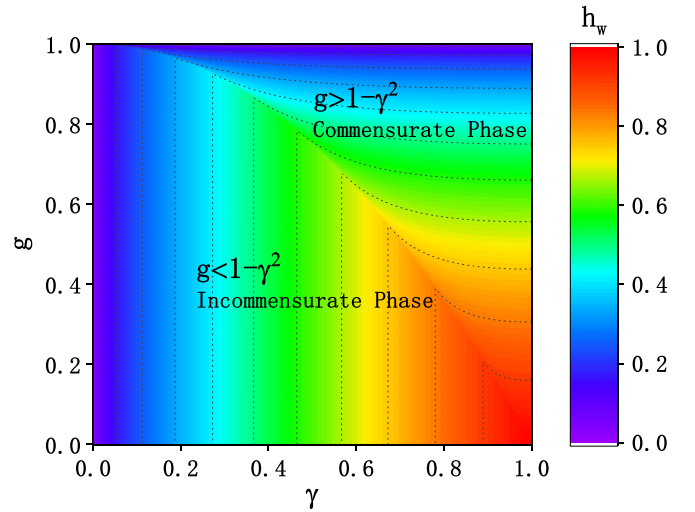


FIG. 5. The trend in the wetting phase transition point  $h_w$  as a function of  $g$  and  $\gamma$ : different colors represent the values of the wetting transition point  $h_w$  for different  $g$  and  $\gamma$ , where  $h_w$  is the boundary between the “wetting” and “nonwetting” phases. The arc representing  $g = 1 - \gamma^2$  is the boundary between the “commensurate” and “incommensurate” phases.

localized states is conditional. They exist only for  $|h_L^x|, |h_R^x| < h_w$ . We solve  $h_w$  by letting  $|x_1| = |x_2| = 1$  in Eq. (19), where the localization length diverges. The detail of the solution on  $h_w$  is given in the Appendix. It is given by

$$\begin{aligned} \text{(a) } g > 1 - \gamma^2, h_{\omega 1} &= \sqrt{\frac{1 - g + \gamma - \sqrt{g(g - 1 + \gamma^2)}}{2}}, \\ \text{(b) } g = 1 - \gamma^2, h_{\omega 2} &= \sqrt{\frac{\gamma(\gamma + 1)}{2}}, \\ \text{(c) } g < 1 - \gamma^2, h_{\omega 2} &= \sqrt{\frac{\gamma(\gamma + 1)}{2}}. \end{aligned} \quad (27)$$

In Eq. (27),  $h_w$  at the wetting phase transition point is equal to  $h_{\omega 1}$  for  $g > 1 - \gamma^2$  and  $h_{\omega 2}$  for  $g \leq 1 - \gamma^2$ .

We present a color map for the relation between  $h_w$  and the parameters  $g, \gamma$  in Fig. 5. The arc represents  $g = 1 - \gamma^2$  and separates the “commensurate” and “incommensurate” phases [33].

For  $|h_L^x| > h_w$  ( $|h_R^x| > h_w$ ), the localized state at the left (right) side of the system vanishes. The continuous wetting transition occurs at this point. In the parameter space we consider, the maximum of  $|h_w|$  is 1 (see the above equation on  $h_w$ ). In order to study the wetting at the left side, we fix  $h_R^x = -1$  to exclude the wetting at the right side. We set  $h_L^x > 0$  and change it around  $h_w$ . It is found that there exists a second-order phase transition for  $g \neq 1 - \gamma^2$  but a fourth-order phase transition for  $g = 1 - \gamma^2$ . For  $h_L^x < h_w$ , a localized state at the left side of the system exists, and the interface is near the left boundary. This phase is called the nonwet phase. Conversely, for  $h_L^x > h_w$ , the interface jumps to the middle of the spin chain. This phase is called the wetting phase [see Fig. 8(a)].

For  $0 < h_L^x < h_w$  and  $h_R^x = -1$ , only one localized state (at the left side) exists. The ground state is given by this localized state. The  $\varepsilon_1$  defined in Eq. (13) is the eigenvalue of this state. The excited states are extended states, for which the eigenvalues satisfy

$$\varepsilon_n = \sqrt{\cos^2 k_n + \gamma^2 \sin^2 k_n - 2g \cos k_n + g^2}. \quad (28)$$

The  $\varepsilon_2$  defined in Eq. (13) is given by the minimum in the above equation.

In light of Eqs. (27) and (28), we obtain the lowest energy of the extended state  $\cos k_1 = \frac{g}{1-\gamma^2}$  for  $g < 1 - \gamma^2$ . Since the wave vector  $k_1$  is not zero, this phase is called incommensurate. For  $g \geq 1 - \gamma^2$ , the lowest energy extended state has  $\cos k_1 = 1$ . This phase is called commensurate.

We can simply show that the energy gap is zero at  $h_L^x = h_w$ . For  $g > 1 - \gamma^2$ , the lowest energy  $\varepsilon_2$  of the extended state is given by Eq. (28) with  $\cos k_1 = 1$ ; it equals  $1 - g$ . The localized state energy  $\varepsilon_1$  at  $h_w$  is given by Eq. (21) with  $x = 1$ , which means an infinitely large localization length. It also equals  $1 - g$ . Therefore the energy gap closes at  $h_L^x = h_w$  for  $g > 1 - \gamma^2$ . For  $g < 1 - \gamma^2$ , the lowest energy of the extended state is given by Eq. (28) with  $\cos k_1 = \frac{g}{1-\gamma^2}$ . The localized state energy is given by Eq. (21) with  $x = \frac{a+i\sqrt{-b}}{c}$  [see Eq. (A5)]. At  $h_L^x = h_w$ , it can be shown that  $\beta = 1 - \gamma^2$ , so it has  $\frac{a}{c} = \frac{g}{1-\gamma^2}$ . With these results, one can show the energy gap is zero at  $h_L^x = h_w$ .

For  $h_L^x > h_w$ , all the eigenvectors are extended states, so the energy gap  $\Delta = \varepsilon_2 - \varepsilon_1 \rightarrow 0$  as the lattice size  $N$  approaches infinity. The system is gapless for  $h_L^x > h_w$ , and gapped for  $h_L^x < h_w$ .

Now we study the scaling of the energy gap for  $h_L^x < h_w$  analytically. The ground state is localized at the left boundary with the energy  $\varepsilon_1$  given by Eq. (21). The first excited state is the extended state with the energy  $\varepsilon_2$  given by Eq. (28), with  $k_n = 0$  for  $g > 1 - \gamma^2$  and  $k_n = g/(1 - \gamma^2)$  for  $g < 1 - \gamma^2$ . The ground state  $\varepsilon_1$  is given by (see the Appendix)

$$g > 1 - \gamma^2, \quad \varepsilon_1 = \sqrt{\frac{4h_L^x{}^2(h_L^x{}^2 - \gamma)(\beta_L^2 - g^2\alpha_L)}{-\beta_L^2\alpha_L}},$$

$$g \leq 1 - \gamma^2, \quad \varepsilon_1 = \sqrt{g^2 + \gamma^2 - \frac{2g\beta_L}{\sqrt{\alpha_L(1-\gamma^2)}} + \frac{\beta_L^2}{\alpha_L}}, \quad (29)$$

where  $\alpha_L$  and  $\beta_L$  are given by Eq. (23).

Considering the critical regime  $h_w - h_L^x \ll 1$ , different relationships between  $g$  and  $1 - \gamma^2$  lead to different values of  $h_w$ , as shown in Eq. (27).

The gap can be described as follows:

$$g > 1 - \gamma^2, \quad \Delta = \zeta_1(h_{w1} - h_L^x)^2 - O(h_{w1} - h_L^x)^3,$$

$$g < 1 - \gamma^2, \quad \Delta = \zeta_2(h_{w2} - h_L^x)^2 + O(h_{w2} - h_L^x)^3, \quad (30)$$

where the coefficients<sup>1</sup>  $\zeta_1, \zeta_2$  only depend on the values of  $g$  and  $\gamma$ .

<sup>1</sup> $\zeta_1 = \frac{-4g^2 - (\gamma+1)(\gamma-1)^2 + g(1-\gamma)(5+3\gamma) + [4g - (1-\gamma)(3+\gamma)]\sqrt{g(-1+g+\gamma^2)}}{(1-g)(\gamma-1)^4(1+\gamma)^2}$   
 $\times 16(1-g-\gamma^2)$  and  $\zeta_2 = \frac{4\gamma(1-g-\gamma^2)}{(1-g)(1-\gamma^2)(\gamma-1)}$ .

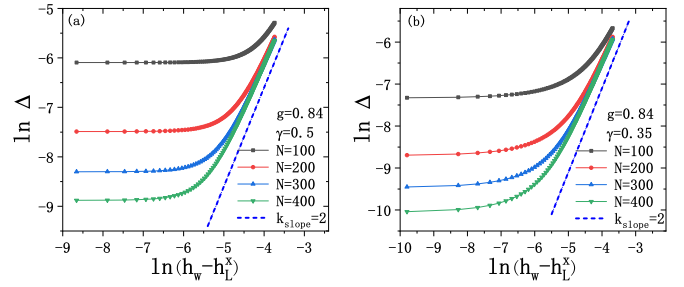


FIG. 6. Finite-size scaling of the energy gap for  $\gamma = 0.5$  and  $0.35$ .

Therefore, the gap  $\Delta$  versus the scaling field  $h_w - h_L^x$  satisfies  $\Delta \sim (h_w - h_L^x)^{z\nu}$  for  $g \neq 1 - \gamma^2$ , and the critical exponent for the energy gap is given by [2]

$$z\nu = 2, \quad (31)$$

where  $\nu$  is the correlation length exponent and  $z$  is the dynamical critical exponent that determines the relative rescaling factors of space and time. Later we will show that  $\nu = 1$ .

Figure 6 shows the log-log plots of the finite-size scaling of the gap  $\Delta$  versus the scaling field  $h_w - h_L^x$ , where the critical exponent for the energy gap is 2 for  $g \neq 1 - \gamma^2$ . It is the same as that for the transverse-field Ising model with boundary fields [27].

We show the boundary magnetization in Fig. 7 for  $\gamma = 0.5, g = 0.84$  where  $g > 1 - \gamma^2$ , and  $\gamma = 0.35, g = 0.84$  where  $g < 1 - \gamma^2$ . And the wetting phase transition occurs at  $h_w = 0.438773\dots$  and  $0.486056\dots$ , respectively, which are obtained from Eq. (27). As we can see, the boundary magnetization is continuous at the transition point  $h_w$ . We also show that the boundary susceptibility  $\chi_1^x$  is defined by

$$\chi_1^x = \frac{\partial m_1^x}{\partial h_L^x}. \quad (32)$$

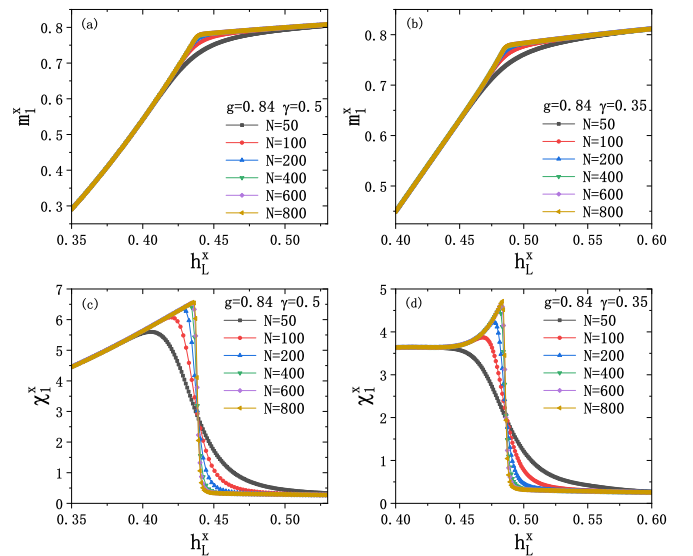


FIG. 7. The boundary (a) magnetization and (c) susceptibility for different lattice sizes with  $g = 0.84, \gamma = 0.5$ . The boundary (b) magnetization and (d) susceptibility for different lattice sizes with  $g = 0.84, \gamma = 0.35$ .

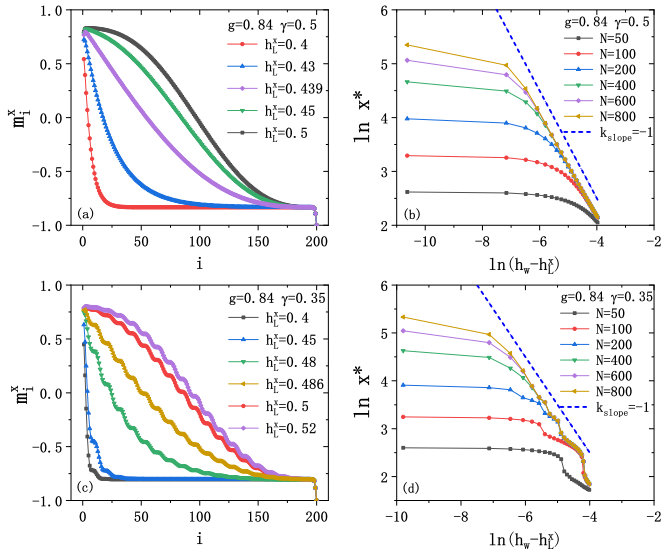


FIG. 8. (a) and (c) Magnetization profiles with different  $h_L^x$  for  $\gamma = 0.5$  and  $0.35$ , respectively. (b) and (d) The wetting layer thickness with different lattices sizes for  $\gamma = 0.5$  and  $0.35$ , respectively. In all cases, the transverse field is set to be  $g = 0.84$ .

It has a jump at the transition point, so the transition is second order. These features are the same as the wetting transition in the transverse-field Ising model [27].

We calculate the magnetization at any site using Eq. (17). Figures 8(a) and 8(c) show the magnetization profile for this XY model with  $N = 200$ ,  $g = 0.84$ ,  $\gamma = 0.5$  and  $0.35$ , respectively. As the boundary fields  $h_L^x > 0$  and  $h_R^x < 0$  have opposite signs, the magnetization profile has an interface at which the magnetization changes sign. The interface is delocalized as  $h_L^x$  approaches the wetting transition point  $h_w$ .

We see that all the curves are smooth for  $g > 1 - \gamma^2$ , which is similar to the result obtained for the one-dimensional transverse-field Ising model [27]. However for  $g < 1 - \gamma^2$ , where the system is in the incommensurate phase, the curves for  $m_i$  versus  $i$  oscillate regularly in Fig. 8(c). This is a reminiscence of  $\cos k = g/(1 - \gamma^2)$  which minimizes  $\varepsilon_n$  in Eq. (28) for  $g < 1 - \gamma^2$ .

We also study the wetting layer thickness  $x^*$  which is the number of spins with positive magnetization. It is finite for  $h_L^x < h_w$  and diverges as  $h_L^x$  approaches  $h_w$ . If  $m_i^x > 0$  and  $m_{i+1}^x < 0$ , the magnetization changes sign between the  $i$ th spin and  $i + 1$ th spin. Therefore the wetting layer thickness is just the position of the interface (where the magnetization is zero). Generally the wetting layer thickness  $x^*$  diverges near the wetting transition point as

$$x^* \sim (h_w - h_L^x)^{-\beta_s}. \quad (33)$$

Figures 8(b) and 8(d) show the divergences of the thickness  $x^*$  and their finite-size scaling for  $g \neq 1 - \gamma^2$ ,

$$\beta_s = 1. \quad (34)$$

However, the curves  $\ln x^*$  versus  $\ln(h_w - h_L^x)$  exhibit some fluctuations due to the oscillation of the magnetization profile for  $g < 1 - \gamma^2$ .

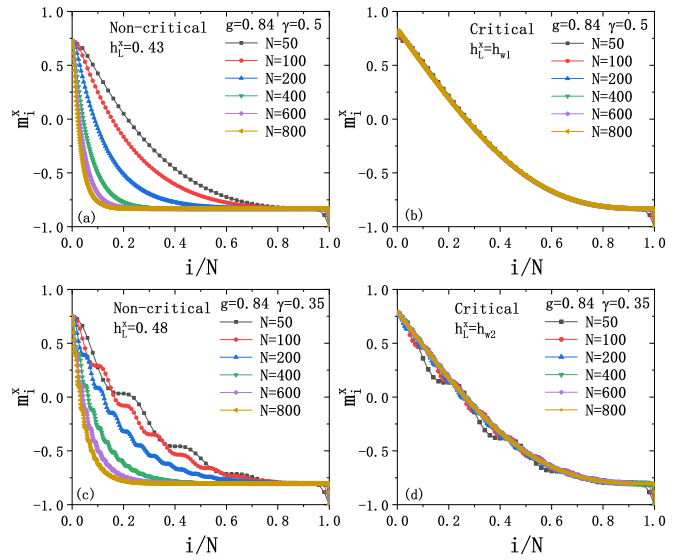


FIG. 9. (a) and (c) Magnetization profile away from the transition point for  $\gamma = 0.5$  and  $0.35$ . (b) and (d) Magnetization profile at the transition point for  $\gamma = 0.5$  and  $0.35$ .

At the transition point  $h_L^x = h_w$  for  $g > 1 - \gamma^2$  and  $g < 1 - \gamma^2$ , the curves for  $m$  versus  $i/N$  collapse for different lattice sizes in Figs. 9(b) and 9(d); however the curves for  $m$  versus  $i/N$  do not collapse for  $h_L^x \neq h_w$ , as shown in Figs. 9(a) and 9(c). And the magnetization at any site fluctuates for  $g < 1 - \gamma^2$ , which is typical for the incommensurate phase. These results show the scale invariance at the phase transition point.

We calculate the correlation function using Eq. (15). Figures 10(a) and 10(c) show the semilog plot for the correlation function  $C_{1,i}^x$  versus  $i$  for different left boundary fields  $h_L^x$  with  $N = 400$ . For  $h_L^x > h_w$ , where the system is in the

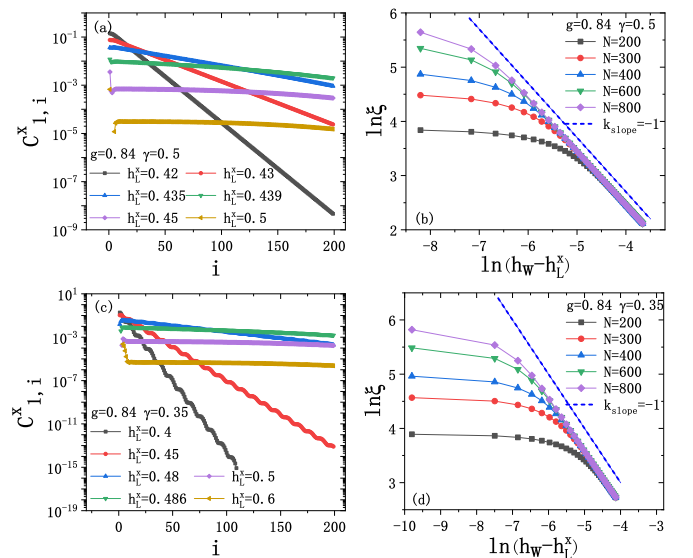


FIG. 10. (a) and (c) Correlation function near the left end with different  $h_L^x$  for  $\gamma = 0.5$  and  $0.35$ , respectively. (b) and (d) Correlation length near the wetting transition point with different size lattices for  $\gamma = 0.5$  and  $0.35$ , respectively.



wetting phase, the correlation of the other spin with the first left boundary field decays rapidly. For  $h_L^x < h_w$ , the system is in the nonwetting phase, and the correlation decays exponentially with the distance from the first spin  $C_{1,i}^x \sim e^{-(i-1)/\xi}$ . Figure 10(c) shows that, especially for  $g < 1 - \gamma^2$ , the correlation decays exponentially with distance from the first spin and also oscillates with the trigonometric function for  $h_L^x < h_w$ .

Next, we choose spins at sites  $i_1$  and  $i_2$ , and calculate the correlation length  $\xi$ :

$$\xi = \frac{i_2 - i_1}{\ln(C_{1,i_1}^x/C_{1,i_2}^x)}. \quad (35)$$

In the numerical calculation, we set  $i_1 = 50$  and  $i_2 = 100$  in Eq. (35). The correlation length diverges near the wetting transition point as follows:

$$\xi \sim (h_w - h_L^x)^{-\nu}. \quad (36)$$

Figures 10(b) and 10(d) show that for  $g \neq 1 - \gamma^2$ , the critical exponent is

$$\nu = 1. \quad (37)$$

According to Eq. (31), it should have

$$z = 2. \quad (38)$$

These exponents  $z, \nu, \beta_s$  are the same as that in the Ising model [27] with boundary fields. They belong to the same universality.

## VI. FOURTH-ORDER PHASE TRANSITION: THE WETTING TRANSITION FOR $g = 1 - \gamma^2$

In this section, we study the phase transition for  $g = 1 - \gamma^2$ . In the numerical calculation, we set  $g = 0.84$  and  $\gamma = 0.4$  where  $g = 1 - \gamma^2$  is satisfied. The wetting phase transition occurs at  $h_w = 0.52915 \dots$  followed from Eq. (27) (b).

For  $g = 1 - \gamma^2$ , there is a localized state  $\varepsilon_1$  given by Eq. (29) and the lowest energy of the extended state  $\varepsilon_2 = 1 - g$  for  $h_R^x < -h_w$  and  $h_L^x \rightarrow h_w$ . We expand the energy gap  $\Delta$  in series of  $h_w - h_L^x$ . The coefficients of the first, second, and third order are all zero. The coefficient of  $(h_w - h_L^x)^4$  is nonzero. The energy gap is given by

$$\Delta = \frac{8}{(\gamma - 1)^3(\gamma + 1)}(h_w - h_L^x)^4 + O(h_w - h_L^x)^5. \quad (39)$$

As shown in Fig. 11, the energy gap diverges at the wetting transition point as  $\Delta \sim (h_w - h_L^x)^4$ , and the critical exponent is [2]

$$z\nu = 4. \quad (40)$$

This critical exponent differs from that for  $g \neq 1 - \gamma^2$  in Eq. (31).

The fourth-order phase transition can be seen from the boundary magnetization, i.e., the order parameter. Figure 12 shows that the boundary magnetization  $m_1^x$  and boundary susceptibility  $\chi_1^x$  are both continuous at the transition point  $h_L^x = h_w = 0.52915 \dots$  for  $g = 0.84$  and  $\gamma = 0.4$ . Figures 12(c) and 12(d) show that the first and second derivatives of the boundary susceptibility  $\chi_1$ , respectively, exhibit regular and

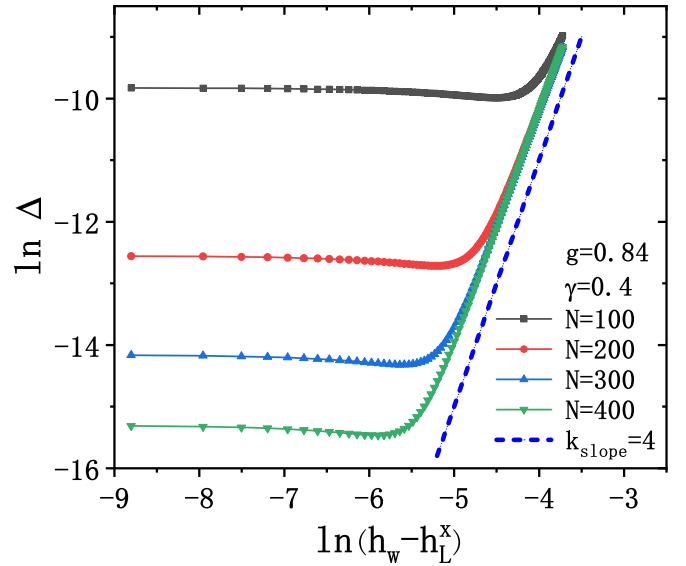


FIG. 11. Finite-size scaling of the energy gap for  $\gamma = 0.4$ .

specific oscillations. The jump in  $\frac{\partial^2 \chi_1^x}{\partial h_L^x^2}$  at  $h_L^x = 0.52915 \dots$  increases with the system size  $N$ , which is a sign for a fourth-order phase transition.

From Fig. 12(d), one can see that the curve of  $\frac{\partial^2 \chi_1^x}{\partial h_L^x^2}$  has a smooth part and an oscillating part. The oscillating parts for different sizes are similar; we conjecture that

$$\frac{\partial^2 \chi_1^x}{\partial h_L^x^2} - f(h_L^x) = \log_{10} N \times \Phi(N\tau_h), \quad (41)$$

where  $\tau_h = (h_L^x - h_w)/h_w$ ,  $\Phi(N\tau_h)$  is the universal scaling function, and  $f(h_L^x) = \lim_{N \rightarrow \infty} \frac{\partial^2 \chi_1^x}{\partial h_L^x^2}$  for  $\tau_h < 0$ , which represents the smooth part of  $\frac{\partial^2 \chi_1^x}{\partial h_L^x^2}$  for  $N \rightarrow \infty$ . The rescaled

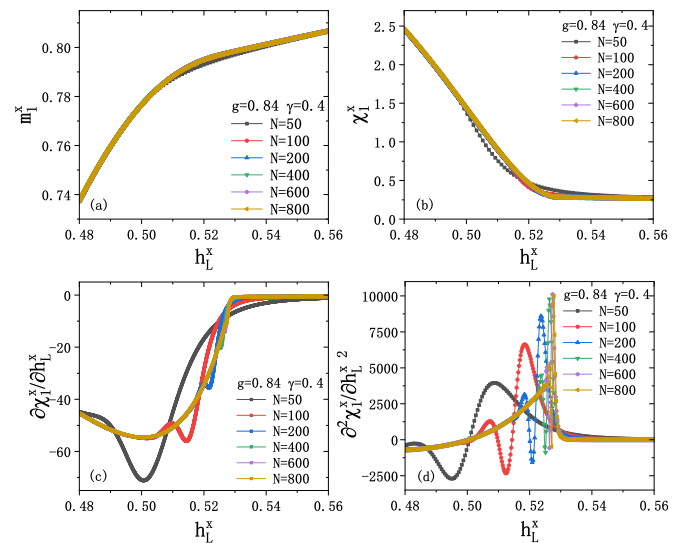


FIG. 12. The boundary magnetization and the boundary susceptibility and its first, second derivatives for different size lattices with  $g = 0.84$  and  $\gamma = 0.4$ .

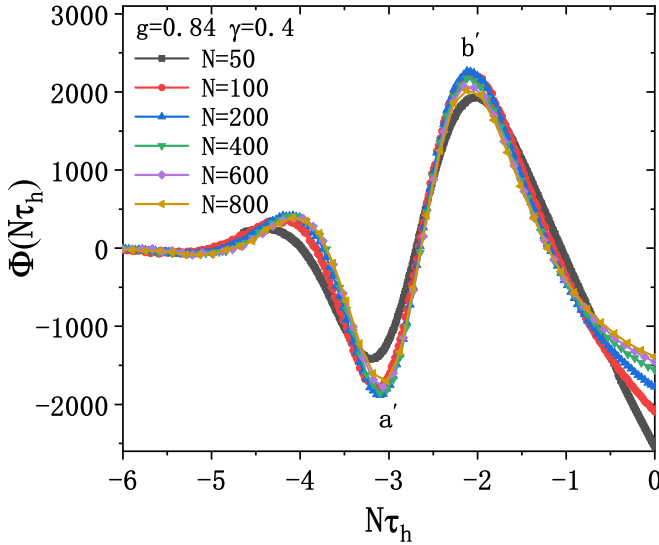


FIG. 13. The data collapse of the rescaled second derivatives of the boundary susceptibility  $\frac{\partial^2 \chi_L^x}{\partial h_L^2}$ .

data for different lattice sizes collapse as shown in Fig. 13. In the limit of  $N \rightarrow \infty$ , the oscillating part is compressed to a range with zero width. This means that the fourth derivative of the energy with respect to the left boundary field is singular. Therefore we call it a fourth-order phase transition.

Figure 14 shows the magnetization profile and wetting layer thickness  $x^*$  for  $g = 1 - \gamma^2$ , where the interface is constantly moving as the boundary field approaches  $h_w$ . In Fig. 14(b), the finite-size scaling of wetting layer thickness  $x^*$  is shown. Obviously it has  $x^* \sim (h_w - h_L^x)^{-\beta_s}$  as  $N \rightarrow \infty$ . We get

$$\beta_s = 1, \quad (42)$$

which is the same as the critical exponent  $\beta_s$  for  $g \neq 1 - \gamma^2$  in Fig. 8.

Figure 15 shows the magnetization profile away from the transition point and at the critical point for  $g = 1 - \gamma^2$ . At the critical point, all the relative magnetization profiles for different size  $N$  coincide. This means that the system is scale free at the critical point. This is another character of critical phenomena.

The correlation functions for  $g = 1 - \gamma^2$  shown in Fig. 16(a) are similar to those for  $g < 1 - \gamma^2$  shown in

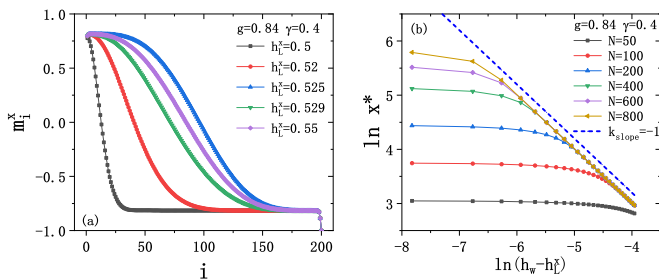


FIG. 14. (a) Magnetization profiles with different  $h_L^x$  for  $g = 0.84$  and  $\gamma = 0.4$ . (b) The wetting layer thickness for lattices with different sizes for  $g = 0.84$  and  $\gamma = 0.4$ .

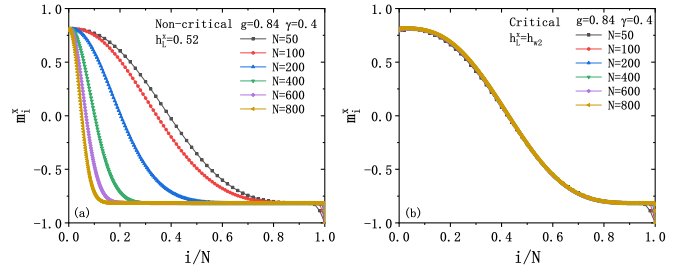


FIG. 15. Magnetization profile for  $g = 1 - \gamma^2$ : (a) away from the transition point and (b) at the transition point.

Fig. 10(c). However, the correlation functions for  $g = 1 - \gamma^2$  fluctuate less frequently as  $h_L^x$  approaches  $h_w$ . This can be understood considering that for  $g > 1 - \gamma^2$ , the incommensurability of the oscillation disappears.

From Fig. 16(b), we get the critical exponent of the correlation length  $\xi$  for  $g = 1 - \gamma^2$ . It is given by

$$\nu = 2. \quad (43)$$

This critical exponent is different from that for  $g \neq 1 - \gamma^2$ . According to Eq. (40), it should have

$$z = 2. \quad (44)$$

The dynamic exponent is the same for the second- and the fourth-order phase transitions.

To further analyze the properties of the correlation function for  $g = 1 - \gamma^2$  and  $g < 1 - \gamma^2$ , we calculate the correlation function  $C_{i,j}^x$  by removing the inflection points in the fluctuation curve for  $h_L^x < h_w$  in Fig. 17, where  $i$  is the position of the first inflection point and  $j$  is the position of the second, third, ... inflection point. The resulting correlation function is smooth and no longer fluctuates. Figure 17(a) shows that the number of inflection points decreases and the distance between two adjacent points increases as  $h_L^x$  approaches  $h_w$  for  $g = 1 - \gamma^2$  with a lattice size  $N = 800$ . For  $g < 1 - \gamma^2$ , the position of the  $j$ th inflection point is almost the same for different  $h_L^x$  in Fig. 17(b).

In this section, we find that the wetting phase transition for  $g = 1 - \gamma^2$  is a fourth-order phase transition. The critical exponent for the energy gap is  $z\nu = 4$  and the correlation length exponent is  $\nu = 2$ .

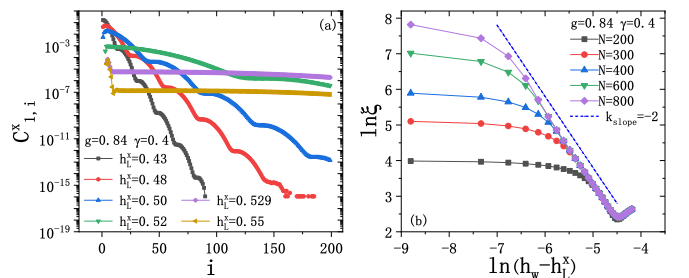


FIG. 16. (a) Correlation function near the left end with different  $h_L^x$  for  $g = 0.84$  and  $\gamma = 0.4$ . (b) Correlation length near the wetting transition point for lattices of different sizes  $N = 200, 300, 400, 600$ , and  $800$  for  $g = 0.84$  and  $\gamma = 0.4$ .

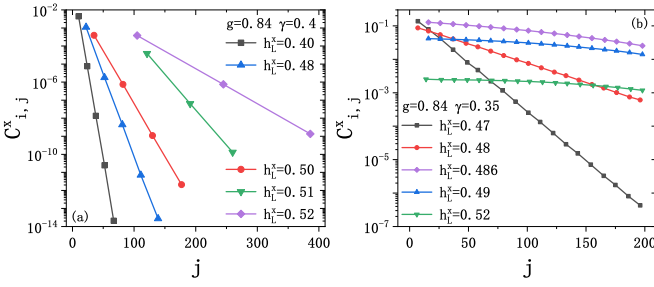


FIG. 17. (a) and (b) Correlation function near the left end obtained by removing the inflection points in the fluctuation curve with different  $h_L^x$  for  $\gamma = 0.4, N = 800$  and  $\gamma = 0.35, N = 400$ , respectively.

For the reader's convenience, we have listed the critical exponents of the transverse-field Ising model and the XY model with different values of  $g$  and  $\gamma$  in Table II; the case  $g \neq 1 - \gamma^2$  was described in Sec. V. In Table II,  $h_{w1}$  and  $h_{w2}$  are given by Eq. (27), and we can see that the wetting phase transition for  $g = 1 - \gamma^2$  belongs to a new universality class.

## VII. THE FINITE-SIZE EFFECT ON THE END POINT OF THE FIRST-ORDER PHASE TRANSITION

In this section, we study the finite-size effect at the end point  $Q$  of the first-order phase transition in the phase diagram Fig. 1. As discussed in Sec. IV, the first-order phase transition occurs at  $h_L = -h_R$  and  $|h_L| = |h_R| < h_w$ , where  $h_w$  is obtained in Sec. V. The end point  $Q$  is at  $h_L = -h_R$  and  $|h_L| = |h_R| = h_w$ . However, this position is valid in the thermodynamic limit, i.e., the system size  $N$  approaching to infinity. For a finite-size system, it is shifted.

In Ref. [29], Parry and Evans discussed a fluid or an Ising magnet confined between two parallel walls that exert different (competitive) boundary fields. Consider a two-dimensional (classical) Ising model with a finite horizontal size  $N$  and an infinite vertical size, and applying opposing fields, say  $h_L, h_R$ , on the left and right boundary (wall), respectively. As we know, in the limit of  $N \rightarrow \infty$ , the system is ordered for  $T < T_{cb}$ , where  $T_{cb}$  is the standard order-disorder critical temperature first found by Onsager [35].

Due to the opposing boundary fields (one favors up-spins and another one favors down-spins), there exists an interface between the opposite magnetization. In this ordered phase, another critical phase transition, the wetting transition, occurs at a temperature  $T_w < T_{cb}$  for the fixed boundaries fields  $h_L, h_R$ , where  $T_w$  depends on the smaller one of the absolute

values of the boundary fields  $|h_L|, |h_R|$  [24,25,36]. Assuming  $|h_L| < |h_R|$ , the wetting transition occurs at the left boundary. For  $T < T_w$ , the interface is localized at the left boundary. For  $T > T_w$ , it is free-energetically favorable for the interface localized in the middle of the system and far away from both boundaries.

For the asymmetric boundary fields, i.e.,  $|h_L| = |h_R|$ , which were just discussed in Ref. [29], the situation is subtle. For  $T < T_w$  the interface can be localized at the left boundary or the right boundary. Both are equally free-energetically favorable. Therefore two phases (one with interface localized at the left boundary and one with interface at the right boundary) coexist. For  $T > T_w$ , there is only one phase even if  $h_L = -h_R$  since the interface is localized at the middle of the system and far away from both boundaries.

The authors in Ref. [29] studied the finite-size effect on the coexistence of two phases within a mean-field analysis. They found that if the fields are such that the fluid wets one wall and dries the other (above a certain critical wetting transition temperature  $T_w$ ), coexistence of two phases, completely wet and completely dry (corresponding to the interface localized at one boundary or another boundary, respectively, in the above discussion on the Ising model), can only occur, for finite wall separation  $N$ , when  $T < T_{c,N}$ , where the critical temperature  $T_{c,N}$  lies below  $T_w$ . The scaling ansatz suggests  $T_w - T_{c,N} \sim N^{-\beta_s}$ , where  $\beta_s$  is the exponent that describes the growth of the wetting layer.

As we know, the fluid or Ising magnet studied in [29] is classical. However, there is a map from the classical liquid-gas phase transition, which belongs to the Ising universality, to the quantum model, the transverse-field Ising model. The quantum phase transition, which is different from the classical phase transition that results from temperature fluctuations, occurs at zero temperature and stems from the quantum fluctuation from the transverse-field term. Therefore the parameter  $g$  plays the role of the temperature  $T$ . In the quantum wetting transition we study, there is a similar finite-size effect, which occurs near the point  $Q$  in Fig. 1.

In Ref. [29], the boundary fields on the two parallel walls are set to be asymmetric, i.e.,  $h_L^x = -h_R^x$ , corresponding to the blue line in Fig. 1, where the first-order phase transition occurs. These two opposite boundary fields produce an interface between the up-spins and down-spins, as the surface fields are competitive. This can be understood as  $h_L$  favoring a liquid (spin-up) and  $h_R$  favoring a gas (spin-down) in Ref. [29]. They found that for  $T < T_{c,N}$ , there are two stable mean-field solutions. These solutions are symmetry-breaking since the interface is localized at the left boundary in one solution and at

TABLE II. A summary of the wetting phase transitions and the critical exponents of the transverse-field Ising model and XY model for different values of  $\gamma$  and  $g$ .

Model	The value of $h_w$	Order of the wetting transition	The critical exponent of			
			Energy gap $\Delta$	Correlation length $\xi$	Thickness $x^*$	Dynamic
Ising model [27]	$\sqrt{1-g}$	Second order	$z\nu = 2$	$\nu = 1$	$\beta_s = 1$	$z = 2$
$g \neq 1 - \gamma^2$	$g > 1 - \gamma^2$ $h_{w1}$	Second order	$z\nu = 2$	$\nu = 1$	$\beta_s = 1$	$z = 2$
	$g < 1 - \gamma^2$ $h_{w2}$	Second order	$z\nu = 2$	$\nu = 1$	$\beta_s = 1$	$z = 2$
$g = 1 - \gamma^2$	$h_{w2}$	Fourth order	$z\nu = 4$	$\nu = 2$	$\beta_s = 1$	$z = 2$

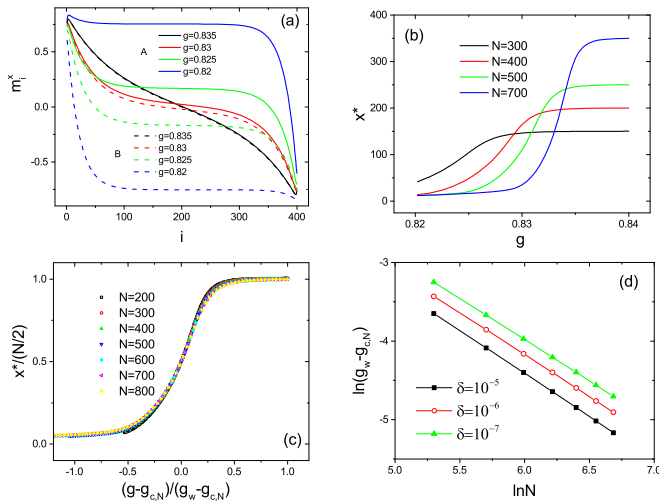


FIG. 18. In all panels,  $\gamma = 1$  is set. (a) The magnetization profiles for different  $g$  with two types of boundary fields. (b) The variation of interface position  $x^*$  with  $g$  under B type boundary condition with different size  $N$ . (c) The collapse of rescaled  $x^*$  and  $g$  for different  $g$  under B type boundary fields. (d) The dependence of  $g_{c,N}$  on the size  $N$  with different  $\delta$ .

the right boundary in another solution (see Fig. 2 in Ref. [29]). For  $T > T_{c,N}$ , there is only one mean-field solution, which is symmetric and the interface is localized just at the middle of the system.

In Fig. 18(a), we show the similar picture in the quantum model. Four groups of magnetization profiles for different  $g$  with  $N = 400$  and  $\gamma = 1$ , which is the Ising case, are calculated. In each group, two types of boundary fields are considered:

$$\begin{aligned} \text{A type: } h_L^x &= h_w + \delta, & h_R^x &= -h_w, \\ \text{B type: } h_L^x &= h_w, & h_R^x &= -h_w - \delta, \end{aligned} \quad (45)$$

where  $\delta$  is very small in order to approach the limit of asymmetric boundary fields  $h_L^x = -h_R^x$ . Practically there is always an environmental noise. Assuming the noise intensity on the boundary fields is  $\delta$ , then the boundary fields can be A type or B type.

For  $\gamma = 1$  the point  $Q$  in Fig. 1 is given by  $h_L^x = -h_R^x = h_w = \sqrt{1-g}$  from Eq. (27). In Fig. 18(a), it is set  $h_w = 0.4$  and  $\delta = 10^{-5}$ . The corresponding  $g$  at the point  $Q$  in Fig. 1 is given by  $g = 1 - h_w^2 = 0.84$ . This gives  $g_w \equiv g_{c,\infty} = 0.84$ , where the quantity  $g_{c,\infty}$  is defined later. The critical point  $g_c$  in the quantum phase transition corresponds to the critical temperature  $T_c$  in Ref. [29]. As one can see, for  $g = 0.835 > g_{c,400}$  ( $= 0.8277043$  in the following), although  $h_L^x, |h_R^x| \lesssim \sqrt{1-g}$ , the profiles for A and B types almost coincide. This corresponds to the region  $T > T_{c,N}$  in Ref. [29], where only one phase can exist. For  $g = 0.825, 0.82 < g_{c,400}$ , and  $h_L^x, |h_R^x| < \sqrt{1-g}$ , as shown in Sec. IV, there exists a positive or negative phase, depending on which boundary field dominates; the profiles for the A and B types are split. These cases correspond to the region  $T < T_{c,N}$  in Ref. [29], where two phases can coexist. The split of A and B type profiles corresponds to the two stable mean-field solutions. However, different from the mean-field calculation in Ref. [29], where

the boundary fields are exactly asymmetric  $h_L^x = -h_R^x$ , the boundary fields in A and B types are almost asymmetric rather than exactly asymmetric. If the boundary fields are set to be exactly asymmetric, i.e.,  $\delta = 0$ , we cannot get the split profiles because of the interference of two degenerated ground states.

This difference between the exact asymmetric boundary fields in Ref. [29] and the almost asymmetric ones in our work can be understood in the following way. Recall the two-dimensional model, where it is disordered for  $T > T_c$  and ordered for  $T < T_c$ . However, if the magnetic field is absent the magnetization is zero in the exact solution because of symmetry. On one hand, only if an infinitesimal magnetic field is introduced, the spontaneous magnetization can be calculated exactly in Yang's seminal work in 1952 [37]. To break the symmetry, an infinitesimal magnetic field is needed in the exact solution. On the other hand, a mean-field solution on this problem can lead to a nonzero spontaneous magnetization below critical temperature without a magnetic field. To break the symmetry, the magnetic field is not needed in the mean-field solution. In Ref. [29], the analysis is mean field, so two stable symmetry-breaking solutions are obtained even with the exactly asymmetric boundary fields. Our solution is (numerically) exact, so the boundary fields can not be exactly asymmetric in the symmetry-breaking solutions.

The A and B profiles are asymmetric. To study their splitting with  $g$ , we calculate the interface position  $x^*$ , where the magnetization is zero for B type boundary fields. The results for  $N = 300, 400, 500, 700$  are shown in Fig. 18(b). The interface position  $x^*$  decreases with  $g$ . At higher  $g$  side, it has  $x^* \approx N/2$ , where A and B type profiles almost coincide. They are not split. At lower  $g$  side, it has  $x^* \ll N/2$ , where A and B type profiles are split radically.

We let

$$x^*(g_{c,N}) = N/4 \quad (46)$$

be the transition point from the coinciding profiles to splitting profiles. For example, we get  $g_{c,300} = 0.8231883$ ,  $g_{c,400} = 0.8277043$ ,  $g_{c,500} = 0.830375$  from the data in Fig. 18(b). We find that  $g_{c,N}$  approaches closer to  $g_w$  for  $N \rightarrow \infty$ ; this point corresponds to  $T_{c,N}$  in Ref. [29]. At first, the minimum of  $x^*$  for B type profiles is zero and the maximum of it is  $N/2$ , so it is natural to let  $x^*$  equal half of its maximum at the transition point. More important, this definition induces the following well defined scaling relations.

It is found that the variations of  $x^*$  vs  $g$  for different size  $N$  can be rescaled with

$$\frac{x^*}{N/2} = X\left(\frac{g - g_{c,N}}{g_w - g_{c,N}}\right), \quad (47)$$

where  $X$  is a universal function and  $g_w$  is the wetting transition point following from Eq. (27) with  $\gamma = 1$ :

$$g_w \equiv g_{c,\infty} = 1 - h_w^2. \quad (48)$$

From the aforementioned discussion, we know that  $g_{c,\infty} = 0.84$  for  $h_w = 0.4$ . The data collapse for  $N = 200, 300, 400, 500, 600, 700, 800$  are shown in Fig. 18(c). The original data for  $N = 300, 400, 500, 700$  are shown in Fig. 18(b).



Moreover, it is found that

$$g_w - g_{c,N} \sim N^{-1/\beta_s}, \quad (49)$$

where  $\beta_s$  the exponent to describe the divergence of wetting layer thickness. From Eq. (34), we know  $\beta_s = 1$ . So we have  $g_w - g_{c,N} \sim N^{-1}$ . The above scaling relation is consistent with the scaling relation  $T_w - T_{c,N} \sim N^{-1/\beta_s}$  in Ref. [29]. The evidence of this scaling relation is shown in Fig. 18(d). In Fig. 18(d), three cases of  $\delta = 10^{-5}, 10^{-6}, 10^{-7}$  are calculated. Although  $g_{c,N}$  depends on the value of  $\delta$ , the dependence of  $\ln(g_w - g_{c,N})$  on  $\ln N$  for the same  $\delta$  is linear obviously. The slopes are  $-1.093(3), -1.062(3), -1.047(3)$  for  $\delta = 10^{-5}, 10^{-6}, 10^{-7}$ , respectively.

We have not studied this effect for the XY model, especially for the fourth-order phase transition with  $g = 1 - \gamma^2$ . This is waiting for future work.

### VIII. SUMMARY

In summary, we have obtained the phase diagram of the transverse-field XY model with boundary fields along the  $x$  direction. First-, second-, and fourth-order phase transitions exist.

The first-order phase transition between positive and negative phases occurs at  $-h_w < -h_R^x = h_L^x < h_w$ , which is the coexistence line. For  $h_R^x < -h_w$  and  $h_L^x = h_w$ , there is a continuous wetting transition. It is second order for  $g \neq 1 - \gamma^2$  and fourth order for  $g = 1 - \gamma^2$ . The second-order wetting transition belongs to the same universality of the transverse-field Ising model with the boundary field. The fourth-order wetting transition belongs to a new universality class, with a correlation length exponent  $\nu = 2$  and a dynamic exponent  $z = 2$ .

Tuning the boundary fields should be simple in the experimental realization. Our work may be tested in further experiments with cold atoms [38].

### ACKNOWLEDGMENTS

This work was supported by the National Natural Science Foundation of China under Grant No. 12175015. The authors acknowledge support extended by the Super-Computing Center of Beijing Normal University.

### APPENDIX: DETERMINATION OF THE PHASE TRANSITION POINT $h_w$

In light of Eqs. (19) and (21), we expand and simplify the first two terms of the eigenequation  $D\psi_k = \varepsilon_k^2 \psi_k$ :

$$\begin{aligned} c_1 E_1 + c_2 E_2 &= 0, \\ c_1 E_1 F_1 + c_2 E_2 F_2 &= 0, \end{aligned} \quad (A1)$$

where

$$\begin{aligned} E_1 &= x_1^3(1 - \gamma)[1 + \gamma - 2gx_1^{-1} + (1 - \gamma)x_1^{-2}], \\ E_2 &= x_2^3(1 - \gamma)[1 + \gamma - 2gx_2^{-1} + (1 - \gamma)x_2^{-2}], \\ F_1 &= -x_1\{1 - \gamma^2 - 2g(1 + \gamma)x_1^{-1} + [(1 + \gamma)^2 - 4h_L^x]x_1^{-2}\}, \\ F_2 &= -x_2\{1 - \gamma^2 - 2g(1 + \gamma)x_2^{-1} + [(1 + \gamma)^2 - 4h_L^x]x_2^{-2}\}. \end{aligned} \quad (A2)$$

And considering  $\varepsilon^2(x_1) = \varepsilon^2(x_2)$  yields the relationship between  $x_1, x_2$ , and  $h_L^x$ ,

$$x_1, x_2 = \frac{a \pm \sqrt{b}}{c}, \quad (A3)$$

where

$$\begin{aligned} a &= g\alpha_L, \\ b &= \alpha_L[g^2\alpha_L - (1 - \gamma^2)\beta_L^2], \\ c &= \alpha_L\beta_L, \end{aligned} \quad (A4)$$

and  $\alpha_L = (1 + \gamma)^2 - 4h_L^x$ ,  $\beta_L = 1 + \gamma - 2h_L^x$ .

To determine  $h_w = \sqrt{\frac{1-g+\gamma-\sqrt{g(g-1+\gamma^2)}}{2}}$  at the wetting phase transition point, we use the critical condition of  $x = 1$  from Eq. (A3). We then consider the magnitude relationship between  $g$  and  $1 - \gamma^2$  by analyzing three cases for Eq. (27):

(1)  $g > 1 - \gamma^2$ . This is the most common case:  $h_w = \sqrt{\frac{1-g+\gamma-\sqrt{g(g-1+\gamma^2)}}{2}}$ . And assuming  $\gamma = 1$ , we restore the transition point  $h_w = \sqrt{1 - g}$ , which is consistent with the wetting phase transition point obtained in the transverse-field Ising model [27].

(2)  $g = 1 - \gamma^2$ . As the term under the square root sign is zero, we can easily determine that  $h_w = \sqrt{\frac{\gamma(\gamma+1)}{2}}$ .

(3)  $g < 1 - \gamma^2$ . For  $h_L^x = 0$ , we know that  $b = (1 + \gamma)^4[g^2 - (1 - \gamma^2)] < 0$ ,  $a = g(1 + \gamma)^2$ , and  $c = (1 + \gamma)^3$  in Eqs. (A4). Thus, for  $g < 1 - \gamma^2$ , Eq. (A3) becomes

$$x = \frac{a + i\sqrt{-b}}{c}, \quad (A5)$$

and it has a magnitude  $|x| = \frac{1-\gamma}{1+\gamma} < 1$ .

However,  $b$  is still less than zero as  $h_L^x$  increases, and  $b$  cannot become positive until  $h_L^x$  is greater than  $\frac{1+\gamma}{2}$ . Thus,  $x$  is a complex number, and  $|x| < 1$  for  $b < 0$ . As  $|x| = \sqrt{\frac{a^2-b}{c^2}} = 1$ , we obtain the wetting transition point  $h_w = \sqrt{\frac{\gamma(\gamma+1)}{2}}$ , which satisfies  $h_w < \frac{1+\gamma}{2}$ .

Considering Eq. (21), the eigenvalue of the localized eigenstate at the left end is given by

$$\varepsilon_L^2 = \frac{4h_L^x(h_L^x - \gamma)(\beta_L^2 - g^2\alpha_L)}{-\beta_L^2\alpha_L}. \quad (A6)$$

The formula presented above only applies to  $g \geq 1 - \gamma^2$ , considering the particularity of  $x$  for  $g < 1 - \gamma^2$ . This case with  $g < 1 - \gamma^2$  does not satisfy Eq. (A6) but satisfies

$$\varepsilon_L^2 = g^2 + \gamma^2 - \frac{2g\beta_L}{\alpha_L(1 - \gamma^2)} + \frac{\beta_L^2}{\alpha_L}. \quad (A7)$$

Conversely, if we fix the left boundary field  $h_L^x$  and vary the right boundary field  $h_R^x$  to observe the quantum phase transition, we similarly expand and simplify the last two terms of the eigenequations  $D^r\psi_k = \varepsilon_k^2\psi_k$  in Eqs. (20) and (21),

where  $D' = (A - B)(A + B)$ :

$$\begin{aligned} d_1 x_1 (\gamma - 1) E'_1 + d_2 x_2 (\gamma - 1) E'_2 &= 0, \\ d_1 E'_1 F'_1 + d_2 E'_2 F'_2 &= 0, \end{aligned} \quad (\text{A8})$$

where

$$\begin{aligned} E'_1 &= 1 - 2gx_1 + x_1^2 + \gamma(x_1^2 - 1), \\ E'_2 &= 1 - 2gx_2 + x_2^2 + \gamma(x_2^2 - 1), \\ F'_1 &= h_R^x (1 + \gamma_N)^2 - (1 + \gamma)[1 + \gamma - 2gx_1 + (1 - \gamma)x_1^2], \\ F'_2 &= h_R^x (1 + \gamma_N)^2 - (1 + \gamma)[1 + \gamma - 2gx_2 + (1 - \gamma)x_2^2]. \end{aligned} \quad (\text{A9})$$

Then we obtain the relationship between  $x_1$ ,  $x_2$ , and  $h_R^x$ :

$$x_1, x_2 = \frac{a' \pm \sqrt{b'}}{c'}, \quad (\text{A10})$$

where

$$\begin{aligned} a' &= g\alpha_R, \\ b' &= \alpha_R [g^2 \alpha_R - (1 - \gamma^2) \beta_R^2], \\ c' &= (1 - \gamma^2) \beta_R. \end{aligned} \quad (\text{A11})$$

For  $\alpha_R = (1 + \gamma)^2 - 4h_R^x$  and  $\beta_R = 1 + \gamma - 2h_R^x$ , the only difference from  $\alpha_L, \beta_L$  is that  $\alpha_R, \beta_R$  is related to  $h_R^x$ . Considering Eq. (21), the eigenvalue of the localized eigenstate at the right end is given by

$$\begin{aligned} g > 1 - \gamma^2, \quad \varepsilon_R^2 &= \frac{4h_R^x (h_R^x - \gamma)(\beta_R^2 - g^2 \alpha_R)}{-\beta_R^2 \alpha_R}, \\ g \leq 1 - \gamma^2, \quad \varepsilon_R^2 &= g^2 + \gamma^2 - \frac{2g\beta_R}{\sqrt{\alpha_R(1 - \gamma^2)}} + \frac{\beta_R^2}{\alpha_R}. \end{aligned} \quad (\text{A12})$$

Equations (A6), (A7), and (A12) show that the difference in the eigenvalues of the localized states at the two boundaries is determined by the two boundary fields  $h_L^x, h_R^x$ . The calculated wetting phase transition point  $h_w$  is consistent with Eq. (27).

- 
- [1] S. L. Sondhi, S. M. Girvin, J. P. Carini, and D. Shahar, *Rev. Mod. Phys.* **69**, 315 (1997).
- [2] S. Sachdev, *Quantum Phase Transitions* (Cambridge University Press, Cambridge, 1999).
- [3] M. Vojta, *Rep. Prog. Phys.* **66**, 2069 (2003).
- [4] E. Lieb, T. Schultz, and D. Mattis, *Ann. Phys.* **16**, 407 (1961).
- [5] S. Katsura, *Phys. Rev.* **127**, 1508 (1962).
- [6] Yu. A. Fridman and D. V. Spirin, *Eur. Phys. J. B* **31**, 311 (2003).
- [7] A. L. Stella and F. Toigo, *Phys. Rev. B* **17**, 2343 (1978).
- [8] J. Sznajd, *Phys. Rev. B* **52**, 4313 (1995).
- [9] H.-Q. Ding, *Phys. Rev. B* **45**, 230 (1992).
- [10] M. S. Makivic, *Phys. Rev. B* **46**, 3167 (1992).
- [11] R. B. Pearson, *Phys. Rev. B* **16**, 1109 (1977).
- [12] J. Oitmaa and D. D. Betts, *Phys. Lett. A* **68**, 450 (1978).
- [13] J. Oitmaa and D. D. Betts, *Can. J. Phys.* **56**, 897 (1978).
- [14] M. Suzuki and S. Miyashita, *Can. J. Phys.* **56**, 902 (1978).
- [15] G. Gomez-Santos and J. D. Joannopoulos, *Phys. Rev. B* **36**, 8707 (1987).
- [16] C. J. Hamer, J. Oitmaa, and Zheng Weihong, *Phys. Rev. B* **43**, 10789 (1991).
- [17] V. Mukherjee, U. Divakaran, A. Dutta, and D. Sen, *Phys. Rev. B* **76**, 174303 (2007).
- [18] G. Vidal, J. I. Latorre, E. Rico, and A. Kitaev, *Phys. Rev. Lett.* **90**, 227902 (2003).
- [19] J. I. Latorre, E. Rico, and G. Vidal, *Quantum Inf. Comput.* **4**, 48 (2004).
- [20] F. Iglói and R. Juhász, *Europhys. Lett.* **81**, 57003 (2008).
- [21] P. G. de Gennes, *Rev. Mod. Phys.* **57**, 827 (1985).
- [22] D. Bonn, J. Eggers, J. O. Indekeu, J. Meunier, and E. Rolley, *Rev. Mod. Phys.* **81**, 739 (2009).
- [23] K. Binder and D. P. Landau, *Phys. Rev. B* **37**, 1745 (1988).
- [24] D. B. Abraham, *Phys. Rev. Lett.* **44**, 1165 (1980).
- [25] D. B. Abraham, in *Phase Transition and Critical Phenomena*, Vol. 10, edited by C. Domb and J. L. Lebowitz (Academic, London, 1986), p. 1.
- [26] M. Campostrini, A. Pelissetto, and E. Vicari, *J. Stat. Mech.* (2015) P11015.
- [27] K. Hu and X. T. Wu, *Phys. Rev. B* **103**, 024409 (2021).
- [28] K. Hu and X. T. Wu, *Phys. Rev. B* **104**, 134430 (2021).
- [29] A. O. Parry and R. Evans, *Phys. Rev. Lett.* **64**, 439 (1990).
- [30] R. Z. Bariev and I. Peschel, *Phys. Lett. A* **153**, 166 (1991).
- [31] H. Hinrichsen, K. Krebs, and I. Peschel, *Z. Phys. B: Condens. Matter* **100**, 105 (1996).
- [32] U. Bilstein and B. Wehefritz, *J. Phys. A: Math. Gen.* **32**, 191 (1999).
- [33] A. Rosengren, *Phys. Rev. B* **37**, 1950 (1988).
- [34] M. Campostrini, J. Nespolo, A. Pelissetto, and E. Vicari, *Phys. Rev. Lett.* **113**, 070402 (2014).
- [35] L. Onsager, *Phys. Rev.* **65**, 117 (1944).
- [36] K. Binder, D. P. Landau, and A. M. Ferrenberg, *Phys. Rev. E* **51**, 2823 (1995).
- [37] C. N. Yang, *Phys. Rev.* **85**, 808 (1952).
- [38] R. Islam, E. E. Edwards, K. Kim, S. E. Korenblit, C. Noh, H. J. Carmichael, G. D. Lin, L. M. Duan, C. C. J. Wang, J. K. Freericks *et al.*, *Nat. Commun.* **2**, 377 (2011).